Proceedings of the ASME 2024 43rd International Conference on Ocean, Offshore and Arctic Engineering
OMAE2024
June 9-14, 2024, Singapore EXPO, Singapore

OMAE2024-121318

NUMERICAL ANALYSIS OF STRUCTURED SHEET MATERIAL IN FLEXIBLE OSCILLATING WATER COLUMN WAVE ENERGY CONVERTER

Yang Huang[1], Guillermo Idarraga[2], Qing Xiao[1]*, Liu Yang[2], Saishuai Dai[1], Farhad Abad[1], Feargal Brennan[1], Saeid Lotfian[1]
[1] Department of Naval Architecture, Ocean & Marine Engineering, University of Strathclyde, Glasgow, UK
[2] Advanced Composite Group, Department of Mechanical and Aerospace Engineering, University of Strathclyde, Glasgow, UK
*Corresponding author: qing.xiao@strath.ac.uk

ABSTRACT

To improve the power output and reduce the stress levels for Flexible Wave Energy Converters (FlexWECs), a structured material using a sheet of natural rubber with a specific pattern called NR937 is developed in this research. Mechanical characterisation tests are conducted to determine the material properties, and the YEOH hyper-elastic model is employed to capture the nonlinear behaviour of this material. Fluid-structure interaction simulations are performed for a FlexWEC using a CFD-FEA tool. The responses of the Poly-A-OWC model equipped with both the innovative NR937 material and a conventional sheet of Natural Rubber (NR) are compared, and the deformation of flexible membrane, stress distribution, flow field, and power output are all fully explored. The results indicate that at resonance, the deformation amplitude of the flexible membrane using NR937 is increased by 1.3 times compared to that using NR, while the maximum stress increases by only 12%. Additionally, the peak power output of the Oscillating Water Column (OWC) Wave Energy Converter (WEC) utilizing NR937 is approximately 2.6 times higher than that of the WEC using NR. This suggests that structured sheet materials possess potential for improving the performance of FlexWECs, including increasing power output, reducing stress levels in flexible membrane and extending the service life.

Keywords: Flexible OWC WEC, Structured sheet material, Fluid-structure interaction, Computational fluid dynamics.

1. INTRODUCTION

Wave Energy Converters (WECs) are at the forefront of renewable energy technology, harnessing the vast power from the ocean waves. Among various WEC designs, flexible Wave Energy Converters (FlexWECs) have emerged as a promising alternative to conventional rigid-body converters. FlexWECs offer several advantages, including increased efficiency, enhanced reliability, and improved survivability under extreme marine conditions, all while maintaining cost-effectiveness [1]. Given its advantages in capturing and converting wave energy into electricity more effectively, the FlexWEC has attracted increasing attention in recent years.

Flexible structures play a key role in the operation of FlexWECs, primarily serving as the primary movers. Furthermore, Power Take-Off (PTO) systems, often integrated with these structures, utilize technologies like Dielectric Elastomer Generators (DEGs) [1]. The performance of FlexWECs is inherently linked to the dynamic behaviour of these flexible structures, which must exhibit significant deformability and robust stress distribution capabilities under the cyclic loading conditions imposed by ocean waves. Therefore, flexible materials are important for the advancement of FlexWEC technology.

However, the application of flexible materials in FlexWECs poses several challenges due to the demanding mechanical requirements. A seemingly paradoxical requirement is that the flexible material needs to be sufficiently soft to allow substantial deformation for power generation, yet its stiffness should significantly increase beyond a certain deformation threshold to mitigate the risk of structural failure due to excessive deformation. Additionally, these materials must withstand repetitive and dynamic loading while maintaining integrity and efficiency.

In response to the aforementioned challenges, structured sheet materials, consisting of an isohedral pattern of elastic rods, have been developed. These materials are distinguished by providing a tailored mechanical response governed by the pattern's configuration. The response of the structural sheet material is dynamic; as the sheet deforms, its stiffness increases in accordance with the alignment of the rods to the applied force. [2]. This behaviour enables structured sheets to provide enhanced deformability and stress distribution. By customizing

structured sheet materials to meet the deformation demands of FlexWECs, it is possible to optimize converter performance significantly.

Structured materials with designed architectures can achieve a vast range of linear elastic behaviours. The architecture of these materials allows for large deformation leading to geometric nonlinearities and new properties, which causes the breakdown of the assumptions that deformations are uniform, like homogeneous rubber samples [3-5]. For auxetic and metamaterials most deformations are localized at the hinges (the joints between rods), such that the global response of the material is entirely different from the local behaviour of its constituents [6-10], like what happens with the structured layer introduced in this work. Carefully choosing the geometry of the linked elements makes mechanisms with arbitrarily complex motions central to a wide range of engineering structures, such as foams, random spring networks, levers, linkages, and others [11-13].

While structured sheet materials have been the subject of various studies, their application in the realm of FlexWECs remains unexplored. This study aims to bridge this gap by developing NR937, a structured sheet material made from natural rubber, featuring a specialized pattern that facilitates excellent deformation characteristics under low-stress conditions. To characterize the mechanical behaviour of NR937, mechanical characterisation tests are performed. Furthermore, a fluid-structure interaction (FSI) analysis tool is employed to carry out numerical simulations of a FlexWEC incorporating this newly developed material [14]. This tool was successfully applied in our previous studies of flexible tube WECs [15, 16].

The present work compares the responses of the Poly-A-OWC model equipped with both the innovative NR937 material and a conventional sheet of natural rubber [17]. From the results, the deformation of the membrane, stress distribution, flow field, and power output are all evaluated, providing insight into the potential performance enhancements offered by structured sheet materials in FlexWECs.

2. NUMERICAL METHOD

2.1 FSI analysis tool

In this study, a FSI analysis tool proposed in the previous work is employed to perform numerical simulations of hydro-elastic responses of FlexWEC with structured sheet materials [14]. This tool is composed of a two-phase Computational Fluid Dynamics (CFD) solver, an open-source three-dimensional (3D) Finite Element Analysis (FEA) code and a multi-physical coupling library.

To predict the 3D transient viscous two-phase flow around the WEC, the continuity equation and incompressible Navier-Stokes (N-S) equations with a laminar model is employed as the governing equations. It should be noted that the compressibility of air and water is ignored in the numerical simulations.

$$\nabla \cdot \mathbf{U} = 0 \tag{1}$$

$$\frac{\partial(\rho \mathbf{U})}{\partial t} + \nabla \cdot \left(\rho(\mathbf{U} - \mathbf{U}_g)\right)\mathbf{U} = -\nabla p_d - \mathbf{g} \cdot x \nabla \rho + \nabla \cdot (\mu \nabla \mathbf{U}) + (\nabla \mathbf{U}) \cdot \nabla \mu + \boldsymbol{f}_\sigma \tag{2}$$

where $\mathbf{U}$ denotes velocity of the flow, $\mathbf{U}_g$ represents the velocity of the mesh grid, ρ signifies the combined mixture density of air and water phases, p_d indicates the dynamic pressure, $\mathbf{g}$ represents the gravity acceleration vector, $\mu = \rho(\nu + \nu_t)$ denotes the dynamic viscosity, ν represents the kinematic viscosity coefficient, ν_t represents the eddy viscosity coefficient, and the term $\boldsymbol{f}_\sigma$ is the surface tension term.

Additionally, the Volume of Fluid (VOF) method is adopted to capture the air-water interface, as referenced in [18]. The core concept of this method involves defining a volume fraction field (α) within each grid cell of the computational domain. The value of the volume fraction signifies the fluid type, as indicated by Eq. (3). Values between 0 and 1 imply that the grid cell is occupied by both water and air, denoting the presence of an interface.

$$\begin{cases} \alpha = 0 \text{ (air)} \\ 0 < \alpha < 1 \text{ (air} - \text{water interface)} \\ \alpha = 1 \text{ (water)} \end{cases} \tag{3}$$

The weak form of the balance of momentum is chosen as the governing equation for solving the structural dynamics of flexible structures, given by:

$$\rho_s \frac{D^2 \mathbf{U_s}}{D^2 t^2} = \nabla \cdot \mathbf{P} + \rho_s \mathbf{f} \tag{4}$$

$$\mathbf{P} = \mathbf{C}\colon \mathbf{E}, \quad \mathbf{E} = \frac{1}{2}(\mathbf{F^T F} - \boldsymbol{\delta}) \tag{5}$$

Here, the symbol ρ_s is indicative of the material density, and $\mathbf{U_s}$ is the vector of displacement. The term $\mathbf{P}$ refers to the second Piola–Kirchhoff stress tensor, while $\mathbf{f}$ corresponds to the forces distributed throughout the body. The elasticity of the material is characterized by the tensor $\mathbf{C}$, and $\mathbf{E}$ signifies the Green–Lagrange strain tensor. Additionally, $\mathbf{F}$ represents the deformation gradient, and $\boldsymbol{\delta}$ is the identity tensor.

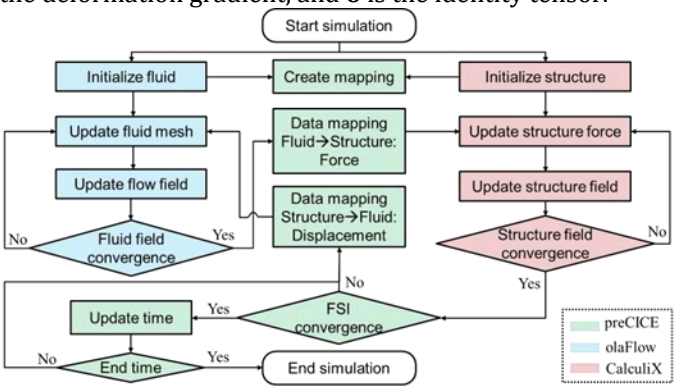

FIGURE 1: FRAMEWORK OF FSI ANALYSIS TOOL [14].

In the present FSI analysis, a two-way strong coupling approach is employed. To guarantee numerical stability and promote convergence, the analysis employs an implicit strategy. Concurrently, the coupling iterations are expedited using an enhanced IQN-IL method [19]. Additionally, node forces from the fluid domain to the solid and vice versa for displacement of vertices are transmitted through an interpolation technique underpinned by radial basis functions (RBF) [20]. The framework of the FSI analysis tool is depicted in Figure 1.

Regarding the damping mechanisms incorporated in the simulation of FlexWEC modelling, the current FSI tool is equipped to account for both fluid damping and structural damping. Damping in flexible oscillating water column (OWC) WECs can fundamentally be classified into two principal categories: damping attributable to viscous losses in the fluid within the submerged section of the OWC duct, and structural damping associated with the deformation of the flexible membrane. In these simulations, the former is naturally integrated during the resolution of the N-S equations, whereas the latter is considered through FEA in the evaluation of membrane deformation.

2.2 Hyper-elastic model

To describe the nonlinear stress-strain characteristics of the structured sheet materials, a hyper-elastic material model is adopted in this study. This model is characterized by a strain energy potential, which is mathematically articulated as follows [21]:

$$E = \sum_{i=1}^{N} C_{i0}(\overline{I_1} - 3)^i + \sum_{i=1}^{N} \frac{1}{D_i}(J-3)^{2i} \qquad (6)$$

Here, I_1 signifies the modified first invariant of the Cauchy-Green deformation tensor, while C_i and D_i are material constants ascertained through experimental results.

3. PROBLEM DESCRIPTION

3.1 Poly-A-OWC model

The flexible OWC WEC model employed in this study is taken from wave tank experiments conducted by Moretti et al., depicted in Figure 2(a) [17]. The model, referred to as the Poly-A-OWC, features a bottom-fixed OWC collector and is capped by a circular flexible membrane. An air chamber is situated between the membrane and the OWC collector. The membrane has a diameter of 400 mm and a thickness of 2 mm. Different with the experimental setup, no pre-stretching of the membrane is incorporated in the numerical simulations to maintain numerical stability. Detailed dimensions of the OWC model are available in Figure 2(b).

Additionally, the air is assumed to be incompressible in this study. Utilizing the ideal gas law, we can estimate the change in air volume of the air chamber after pressure changes with the following formula [22]:

$$v = v_0 \left(\frac{p_a}{p_a + p}\right)^{1/\gamma} \qquad (7)$$

where v denotes the air volume under pressure p, v_0 represents the initial air volume, p_a represents the atmosphere pressure, and γ =1.4 is the specific heat ratio for air. Based on our numerical results, the maximum pressure amplitude in the air chamber is approximately 1760 Pa, leading to the largest change in air volume within the air chamber of about 1.2%, which can be ignored in the simulation.

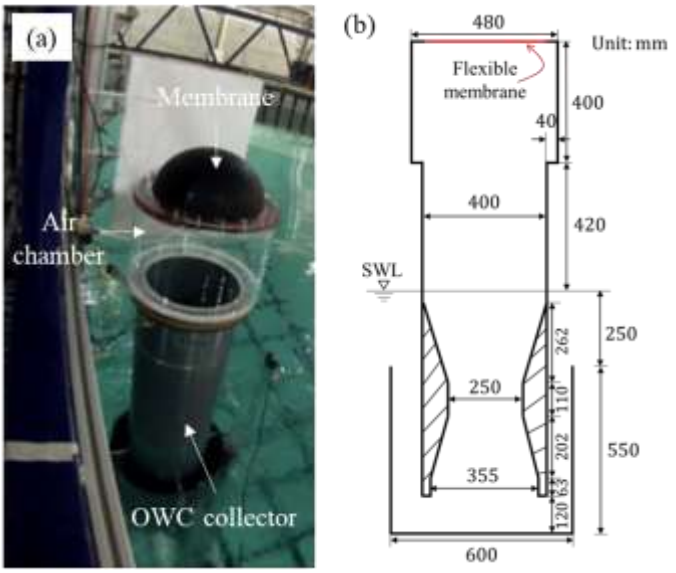

FIGURE 2: GEOMETRIC MODEL OF POLY-A-OWC WEC: (a) EXPERIMENTAL SET UP; (a) GEOMETRIC DIMENSIONS [17].

3.2 Structured sheet material

To enhance the power output of the flexible OWC WEC while simultaneously reducing the risk of failure in the flexible membrane, an increase in the membrane's deformation is required, alongside a mitigation of the stresses within it. In this regard, we have developed a structured sheet material using a sheet of Natural Rubber (NR) with a specific pattern, termed NR937, as illustrated in Figure 3(a). The pattern exhibits significantly lower stiffness compared to conventional NR sheet at low stress levels. Owing to its distinct patterned construction, the structured sheet displays a progressive increase in stiffness in response to escalating stress levels. NR937 allows for greater deformation under lower external forces, with correspondingly reduced stress levels, thereby enhancing the performance of flexible WECs. Conversely, under higher external forces, NR937 exhibits reduced deformation, which serves to prevent failure in the flexible membrane.

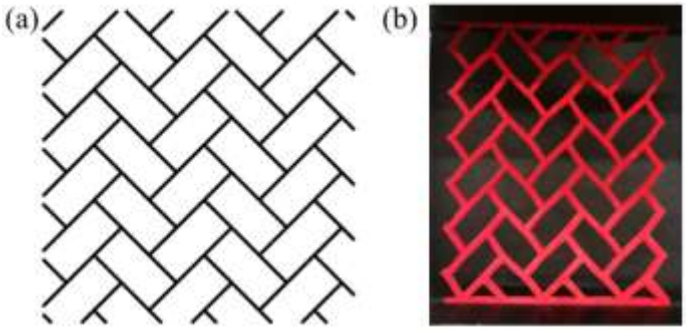

FIGURE 3: (a) PLANNAR TESTS FOR FLEXIBLE MATERIAL NR937; (a) STRUCTUED SHEET WITH PATTERN 937.

To determine the material properties of NR and NR937, they were characterized under uniaxial loading conditions using a computer-controlled Testometric 500X-50 universal servo-

electric testing machine, as illustrated in Figure 3(b). Hyperelastic constants were derived for incorporation into the numerical model by fitting the Yeoh model within ABAQUS. This process utilized a strain energy potential of third order and assumed material incompressibility. This methodology has been successfully applied in determining the material properties of flexible materials in our previous research [23]. Table 1 provides a summary of the hyperelastic constants of the Yeoh model implemented in the simulations. The fitted stress-strain curves for NR and NR937 are showcased in Figure 4.

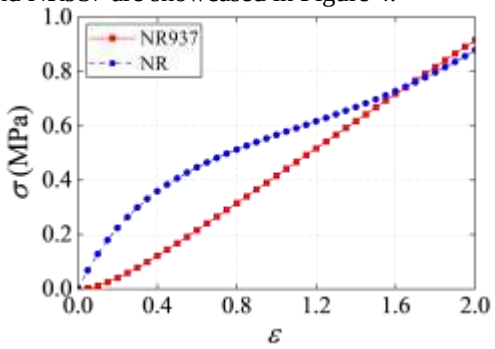

FIGURE 4: STRESS-STRAIN CURVES OF NATURAL RUBBER (NR) AND STRUCTURED SHEET MATERIAL (NR937).

It is important to clarify that the stress-strain characteristics obtained from planar testing reflect the material properties in a uniaxial direction, which may not accurately represent the complex material behaviour of an anisotropic material like NR937 during deformation for the flexible OWC WEC. Consequently, for the purposes of numerical simulation, we employ an isotropic, homogenous, and solid flexible material whose hyper-elastic constants are assumed to be equivalent to those of NR937. The above factors will be further considered in a separate journal paper.

TABLE 1: HYPER-ELASTIC CONSTANTS OF NR AND NR937.

Material	C_{10} (MPa)	C_{20} (MPa)	C_{30} (MPa)
NR	2.40E-01	-4.14E-03	1.83E-04
NR937	3.63E-02	2.50E-02	-1.64E-03

3.3 Computational set up

A shown in Figure 5, a cuboid region with the dimensions of 3.4 m × 2 m × 3.5 m is constructed for the simulation. The FlexWEC model is positioned at the centre of the domain. The water depth is set to 2 m. Watch points are established to record the pressure within the air chamber and the water level in the OWC collector. The incident wave conditions are modelled using regular waves defined by the Stokes second-order wave theory, with wave parameters detailed in Table 2.

The boundary conditions are defined as follows: The inlet boundary is prescribed with a velocity condition defined by the incident waves, whereas the outlet boundary is set to a zero gradient condition to simulate an open boundary. The top boundary is treated with a slip condition, and the bottom boundary adopts a wall condition to reflect the seafloor. The front and back boundaries are assigned a symmetric condition.

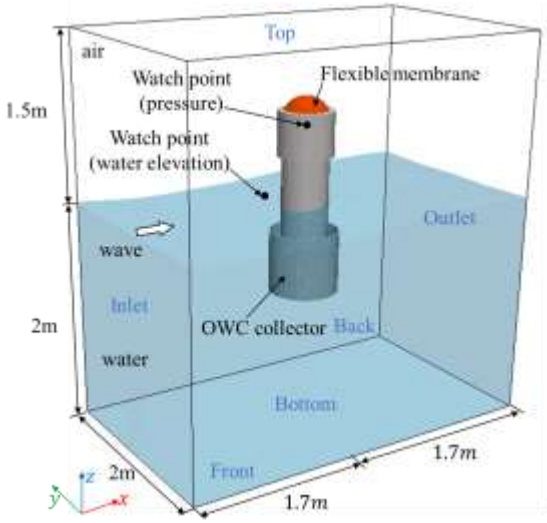

FIGURE 5: COMPUTATION DOMAIN.

TABLE 2: WAVE CONDITIONS.

Wave parameters	Wave frequency f_w (Hz)	Wave period T_w (s)	Wave height A_w (m)
Value	0.3~0.85	1.18~3.33	0.05

3.4 Grid and time step convergence test

To determine the proper grid size for the numerical simulation, a grid convergence test was conducted. Three different mesh resolutions were evaluated: the coarse mesh featured a minimum face mesh size of 0.012m×0.012m on the membrane, which was about 3% of the membrane's diameter. For the medium mesh, this size was reduced to 2% of the membrane diameter, and further decreased to 1.3% for the fine mesh. The time history of the midpoint displacement of the flexible membrane under varying mesh resolution is presented in Figure 6. The results predicted by medium mesh and fine mesh are very close to each other, thus the medium mesh is chosen for the following simulations to reduce the computational cost. Regarding the time step size, a value of 2e-3s, approximately 1/588 of the minimum wave period, has been chosen to ensure the stability of the FSI simulation. Previous experience suggests that this level of time step granularity is adequate for obtaining converged results in the simulation.

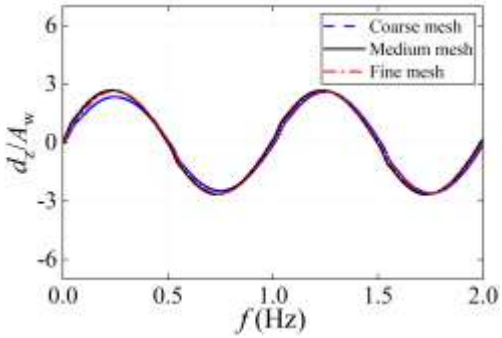

FIGURE 6: TIME HISTORY OF THE MIDPOINT DISPLACEMENT OF THE FLEXIBLE MEMBRANE UNDER VARYING MESH RESOLUTION.

4. RESULTS AND DISCUSSIONS

In this section, the results are presented, beginning with the interaction between the fluid and the flexible membrane, which includes variations of the wave elevation, pressure field and membrane deformation. Subsequently, the study evaluates the amplitude of pressure within the air chamber and the deformation amplitude of the membrane across different wave frequencies to investigate the impact of structured sheet materials. Furthermore, an analysis is conducted on the structural behaviour of the membrane when integrated with structured sheet materials, focusing on deformation and stress distribution. The discussion also extends to the power output performance of the flexible OWC WEC, highlighting its operational efficiency.

4.1 Fluid-flexible membrane interaction

For a better understanding of the interactions between fluid dynamics and the flexible membrane within OWC WEC, we focus on a representative case study. This scenario employs the structured sheet material NR937 at a resonant frequency of f_w = 0.6 Hz. Figure 7 displays four snapshots of the fluid field within a single wave period. Here, the water surface is represented by varying colours to indicate elevation levels, while the pressure contours delineate the internal fluid dynamics within the OWC collector. Uniform pressure distribution is observed within the air chamber. Thus, a watch point is positioned beneath the midpoint in the air chamber to monitor pressure changes, complemented by wave probes that record the water elevation both inside the OWC collector and in the surrounding wave environment, as depicted in Figure 5.

Figure 8 depicts the temporal variation of wave elevation within the OWC collector (η) in comparison to the external wave elevation (η_0). Both elevations exhibit periodic variation over time, with the phase of η_0 leading η by 90 degrees. The pressure within the air chamber, subject to the influence of the OWC beneath, varies significantly over time, which is illustrated in Figure 9. The resulting pressure fluctuations prompt cyclical deformations of the flexible membrane, oscillating both upwards and downwards, as illustrated in Figure 10. It is noted that the water elevation in the OWC collector, the pressure in the air chamber, and the deformation of the membrane are all in phase, demonstrating a synchronized system response.

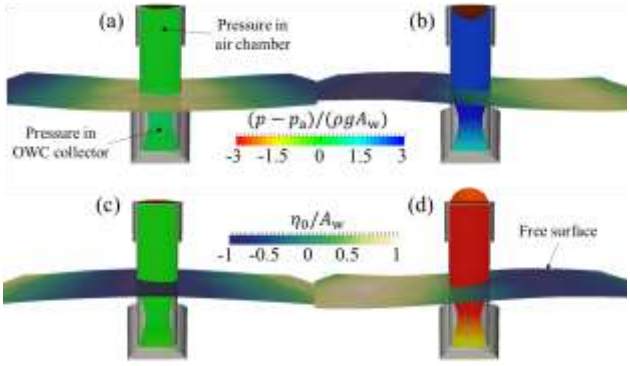

FIGURE 7: INSTANTANEOUS FLOW FIELD OF FLEXIBLE OWC WEC USING NR937 WITHIN ONE WAVE PERIOD: (a) $t = 0\ T_W$; (b) $t = 0.25\ T_W$; (c) $t = 0.5\ T_W$; (d)$t = 0.75\ T_W$ (T_w = 1.67 s).

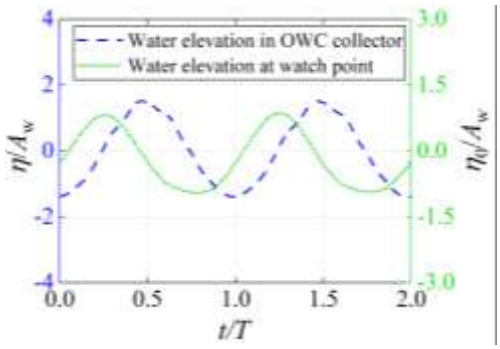

FIGURE 8: TIME HISTORY OF WATER ELEVATION (η) IN OWC COLLECTOR AND THE WATER ELEVATION (η_0) AT THE WATCH POINT (NORMALIZED BY WAVE AMPLITUED A_W) (f_w = 0.6 Hz).

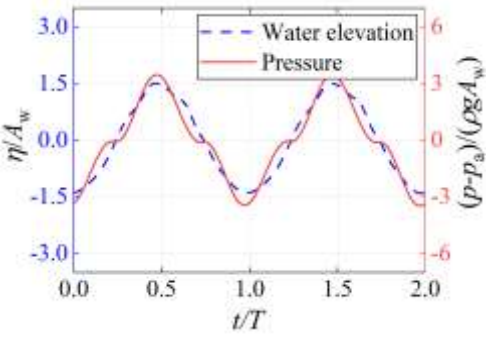

FIGURE 9: TIME HISTORY OF WATER ELEVATION η (NORMALIZED BY WAVE AMPLITUED A_W) IN THE OWC COLLECTOR AND PRESSURE p-p_a (NORMALIZED BY $\rho g A_W$, p_a IS THE STANDARD ATMOSPHERIC PRESSURE) IN THE AIR CHAMBER (f_w = 0.6 Hz).

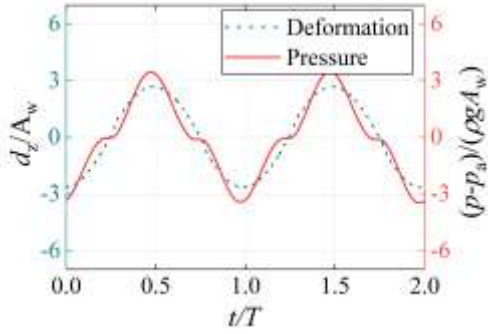

FIGURE 10: TIME HISTORY OF DISPLACEMENT AMPLITUDE d_Z (NORMALIZED BY WAVE AMPLITUED A_W) OF THE MIDPOINT ON THE FLEXIBLE MEMBRANE AND PRESSURE p-p_a (NORMALIZED BY $\rho g A_W$, p_a IS STANDARD ATMOSPHERIC PRESSURE) IN THE AIR CHAMBER (f_w = 0.6 Hz).

To investigate the impact of structured sheet material, this study quantifies the pressure amplitude in the air chamber (A_p) and the deformation amplitude of the flexible membrane (A_d) using NR937 across a range of wave frequencies. These results are compared with outcomes obtained from employing natural rubber (NR), as depicted in Figures 11 and 12. It is observed that

both A_p and A_d achieve their maximal values at a wave frequency of 0.6 Hz with NR937, denoting the resonant frequency of the FlexWEC. This resonant frequency rises to 0.8 Hz when the membrane is composed of NR. This shift is primarily due to the significantly reduced stiffness of NR937 compared to NR at low-pressure conditions. Furthermore, the peak A_p with an NR937 membrane is approximately 25% greater than that with an NR membrane, while the maximum A_d with NR937 is around 2.3 times that of NR. This indicates a nonlinear correlation between pressure amplitude and membrane deformation.

Moreover, when assessed at a wave frequency of 0.35 Hz, the A_p observed with an NR937 membrane is roughly 76% of the amplitude seen with a NR membrane, and the A_d with NR937 is approximately 188% of that recorded with NR. These results effectively highlight the advantages of structured sheet materials and underscore the rationale behind their development: to facilitate substantial deformations under low-pressure conditions, thereby potentially enhancing power output and electrical energy generation.

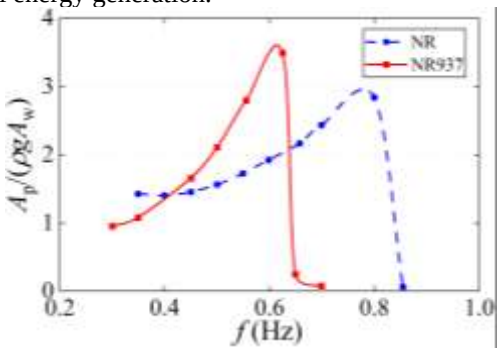

FIGURE 11: PRESSURE AMPLITUDE A_p (NORMALIZED BY $\rho g A_W$) IN THE AIR CHAMBER UNDER VARIOUS WAVE FREQUENCIES.

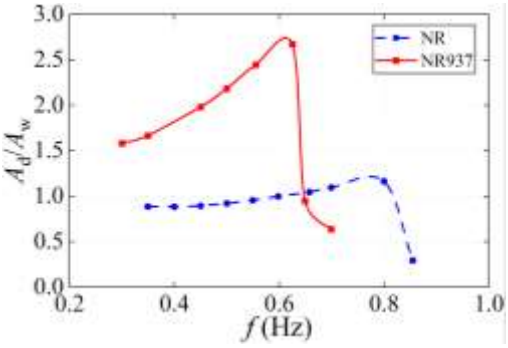

FIGURE 12: DEFORMATION AMPLITUDE A_d (NORMALIZED BY WAVE AMPLITUED A_w) OF THE FLEXIBLE MEMBRANE UNDER VARIOUS WAVE FREQUENCIES.

4.2 Structural responses of flexible membrane

As mentioned above, the maximum deformation of the flexible membrane using NR937 at the resonant frequency is considerably greater than that of NR. To clearly illustrate the deformation of the flexible membrane, Figure 13 compares the maximum deformations observed with both NR and NR937 materials. The membrane deformation exhibits radial symmetry. A larger deformation is typically accompanied by increased stress, as evidenced in Figure 14, which displays the stress distribution on the membranes at their maximum deformation. It is observed that the stress is highest at the edges of the membrane. Although most regions of the membrane with NR937 exhibit higher stress levels compared to those with NR, the maximum stresses between the two are relatively similar.

To quantify this difference, the peak stresses on the membranes with NR937 and NR across various wave frequencies are plotted in Figure 15. Interestingly, the maximum stress on the membrane using NR937 is only 12% higher than that with NR. This increment is modest compared to the 1.3 times increase in deformation amplitude (A_d). This underscores the superiority of structured sheet materials, where the increase in stress is much smaller than the increase in deformation amplitude, benefiting the structural life and reducing the failure of flexible membrane.

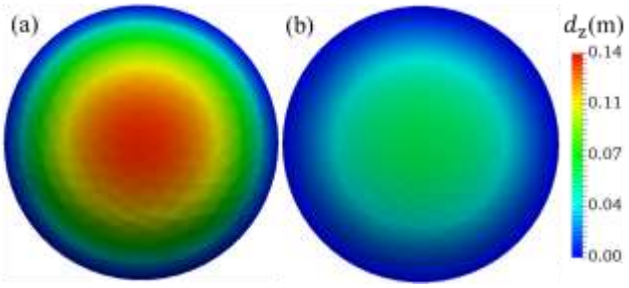

FIGURE 13: MAXIMUM DEFORMATION OF THE FLEXIBLE MEMBRNAE: (a) NR937 (f_W = 0.6 HZ); (b) NR (f_w = 0.8 Hz).

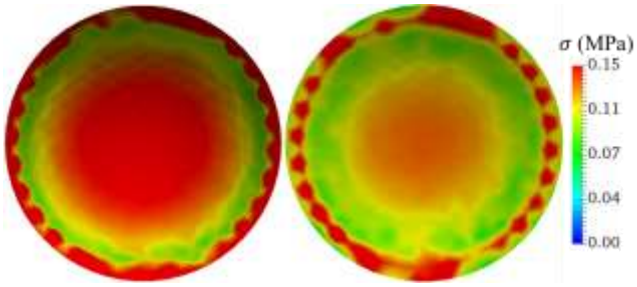

FIGURE 14: STRESS DISTRIBUTION ON THE FLEXIBLE MEMBRANE UNDER MAXIMUM DEFORMATION: (a) NR937 (f_W = 0.6 HZ); (b) NR (f_w = 0.8 Hz).

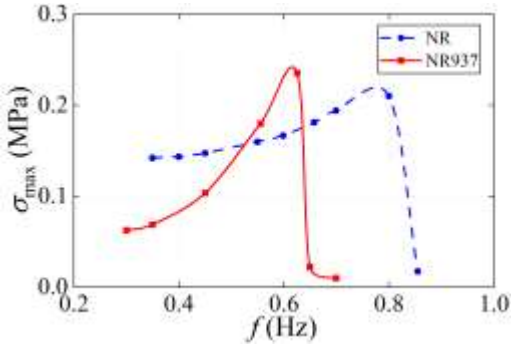

FIGURE 15: MAXIMUM STRESS ON THE FLEXIBLE MEMBRANE UNDER VARIOUS WAVE FREQUENCIES.

4.3 Power output of flexible OWC WEC

To further evaluate the effects of structured sheet material on WEC's power output, we calculate the maximum potential electrical power based on the membrane's deformation.

$$W_{\mathrm{u}} = \frac{1}{2}C_{\mathrm{B}}{V_{\mathrm{B}}}^2 - \frac{1}{2}C_{\mathrm{A}}{V_{\mathrm{A}}}^2 + \frac{1}{2}C_{\mathrm{a}}\left({V_{\mathrm{B}}}^2 - {V_{\mathrm{A}}}^2\right) \quad (8)$$

where W_{u} denotes the electrical energy generated in a cycle, C_{A} and C_{B} represent the capacitance of the flexible membrane at its maximum deformation and in its flat configuration, respectively, V_{A} and V_{B} correspond to the voltages applied to the flexible membrane in these respective states, C_{a} indicates the capacitance of the capacitor in parallel with the flexible membrane. For an in-depth explanation of this power calculation methodology, the study by Moretti et al. [14, 24] can be consulted.

Figure 16 shows the estimated power generation of the 1:30 WEC model over a spectrum of wave frequencies. Notably, that the power output when employing NR937 exceeds that of NR at wave frequencies below 0.65 Hz. Moreover, the peak power output with NR937 is approximately 2.6 times greater than that with NR. Extrapolating these results to the full-scale model, based on the current scale ratio of 1:30, the substitution of NR with NR937 could potentially elevate the output power of the WEC from 103 kW to 268 kW under full-scale conditions. This indicates a significant improvement in energy conversion efficiency through the utilization of structured sheet material.

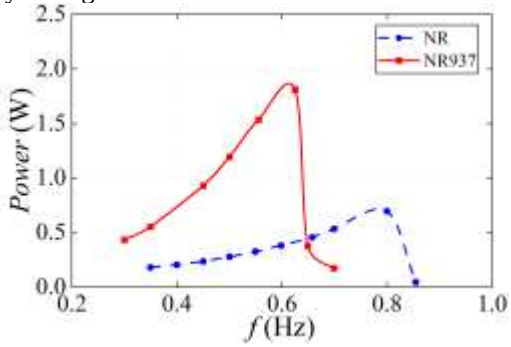

FIGURE 16: ESTIMATED POWER OUTPUT OF THE FLEXIBLE OWC WEC (MOEDL SCALE 1:30) UNEDR VARIOUS WAVE FREQUENCIES.

5. CONCLUSION

In this study, we developed a structured sheet material, NR937, to improve the power output and reduce the stress levels in flexible OWC WEC. Material properties were determined through planar loading tests, and the nonlinear behaviour of the materials was captured using the YEOH hyper-elastic model. FSI responses of the WEC were analysed, considering the influence of the structured sheet material.

The distinctive feature of NR937 is its variable stiffness with strain: it exhibits low stiffness at low strains and high stiffness at high strains. Under minimal external forces, the flexible membrane composed of NR937 can undergo substantial deformation with minimal stress, which is advantageous for achieving higher power output and reducing fatigue loading. Conversely, under substantial external forces, the increased stiffness of NR937 helps to prevent excessive deformation of the flexible membrane, thereby mitigating the risk of failure. The results indicate that at resonance, the deformation amplitude of the flexible membrane using NR937 is increased by 1.3 times compared to that using NR, while the maximum stress increases by only 12%. Additionally, the peak power output of the OWC WEC utilizing NR937 is approximately 2.6 times higher than that of the WEC using NR.

This work contributes to the performance optimization of FlexWECs. It offers a novel approach from the perspective of new material development for enhancing the performance of FlexWECs and demonstrates the benefits of structured sheet materials. However, the structured sheet material used in this investigation is based on isotropic, homogeneous, and solid assumptions. In the future, we plan to manufacture this structured sheet material and conduct wave tank tests to further validate its performance benefits.

ACKNOWLEDGEMENTS

This research was supported by an EPSRC Grant "Bionic Adaptive Stretchable Materials for WEC (BASM-WEC)" (No. EP/V040553/1). This work used the Cirrus UK National Tier-2 HPC Service at EPCC (http://cirrus.ac.uk) funded by the University of Edinburgh and EPSRC (EP/P020267/1).

REFERENCES

[1] Moretti, G., Herran, M. S., Forehand, D., Alves, M., Jeffrey, H., Vertechy, R., & Fontana, M. (2020). Advances in the development of dielectric elastomer generators for wave energy conversion. Renewable and Sustainable Energy Reviews, 117, 109430.

[2] Schumacher, C., Marschner, S., Gross, M., & Thomaszewski, B. (2018). Mechanical characterization of structured sheet materials. ACM Transactions on Graphics (TOG), 37(4), 1-15.

[3] Wyart, M., Liang, H., Kabla, A., & Mahadevan, L. (2008). Elasticity of floppy and stiff random networks. Physical review letters, 101(21), 215501.

[4] Overvelde, J. T., & Bertoldi, K. (2014). Relating pore shape to the non-linear response of periodic elastomeric structures. Journal of the Mechanics and Physics of Solids, 64, 351-366.

[5] Pérez, J., Thomaszewski, B., Coros, S., Bickel, B., Canabal, J. A., Sumner, R., & Otaduy, M. A. (2015). Design and fabrication of flexible rod meshes. ACM Transactions on Graphics (TOG), 34(4), 1-12.

[6] Mullin, T., Deschanel, S., Bertoldi, K., & Boyce, M. C. (2007). Pattern transformation triggered by deformation. Physical review letters, 99(8), 084301.

[7] Overvelde, J. T. B., Shan, S., & Bertoldi, K. (2012). Compaction through buckling in 2D periodic, soft and porous structures: effect of pore shape. Advanced Materials, 24(17), 2337-2342.

[8] Coulais, C., Overvelde, J. T., Lubbers, L. A., Bertoldi, K., & van Hecke, M. (2015). Discontinuous buckling of wide beams and metabeams. Physical review letters, 115(4), 044301.

[9] Zehnder, J., Coros, S., & Thomaszewski, B. (2016). Designing structurally-sound ornamental curve networks. ACM Transactions on Graphics (TOG), 35(4), 1-10.
[10] Konaković, M., Crane, K., Deng, B., Bouaziz, S., Piker, D., & Pauly, M. (2016). Beyond developable: computational design and fabrication with auxetic materials. ACM Transactions on Graphics (TOG), 35(4), 1-11.
[11] Ellenbroek, W. G., Zeravcic, Z., van Saarloos, W., & van Hecke, M. (2009). Non-affine response: Jammed packings vs. spring networks. Europhysics Letters, 87(3), 34004.
[12] O'Rourke, J. (2011). How to fold it: the mathematics of linkages, origami, and polyhedra. Cambridge University Press.
[13] Ellenbroek, W. G., Hagh, V. F., Kumar, A., Thorpe, M. F., & Van Hecke, M. (2015). Rigidity loss in disordered systems: Three scenarios. Physical review letters, 114(13), 135501.
[14] Huang, Y., Xiao, Q., Idarraga, G., Yang, L., Dai, S., Abad, F., Brennan, F., Lotfian, S. (2023). Novel computational fluid dynamics-finite element analysis solution for the study of flexible material wave energy converters. Physics of Fluids, 35(8).
[15] Huang, Y., Xiao, Q., Idarraga, G., Yang, L., Dai, S., Abad, F., Brennan, F., Lotfian, S. (2023, June). Numerical analysis of flexible tube wave energy converter using CFD-FEA method. In Proceedings of the ASME 2023 42nd International Conference on Ocean, Offshore and Arctic Engineering (p. 101302).
[16] Huang, Y., Xiao, Q., Idarraga Alarcon, G., Yang, L., Dai, D., Abad, F., Brennan, F., Lotfian, S. (2023, June). A CFD-FEM analysis for Anaconda WEC with mooring lines. In Proceedings of the European Wave and Tidal Energy Conference (Vol. 15).
[17] Moretti, G., Rosati Papini, G. P., Daniele, L., Forehand, D., Ingram, D., Vertechy, R., & Fontana, M. (2019). Modelling and testing of a wave energy converter based on dielectric elastomer generators. Proceedings of the Royal Society A, 475(2222), 20180566.
[18] Hirt, C. W., & Nichols, B. D. (1981). Volume of fluid (VOF) method for the dynamics of free boundaries. Journal of computational physics, 39(1), 201-225.
[19] Degroote, J., Bathe, K. J., & Vierendeels, J. (2009). Performance of a new partitioned procedure versus a monolithic procedure in fluid–structure interaction. Computers & Structures, 87(11-12), 793-801.
[20] Lindner, F., Mehl, M., & Uekermann, B. (2017). Radial basis function interpolation for black-box multi-physics simulations.
[21] Martins, P. A. L. S., Natal Jorge, R. M., & Ferreira, A. J. M. (2006). A comparative study of several material models for prediction of hyperelastic properties: Application to silicone‐rubber and soft tissues. Strain, 42(3), 135-147.
[22] Vertechy, R., Fontana, M., Papini, G. R., & Forehand, D. (2014, March). In-tank tests of a dielectric elastomer generator for wave energy harvesting. In Electroactive Polymer Actuators and Devices (EAPAD) 2014 (Vol. 9056, pp. 332-342). SPIE.
[23] Idarraga, G., Yang, L., Abad, F., Huang, Y., Dai, S., Xiao, Q., Lotfian, S., Brennan, F. (2023, June). Hyperelastic modelling of elastomers for wave energy convertors. In International Conference on Offshore Mechanics and Arctic Engineering (Vol. 86854, p. V003T03A001). American Society of Mechanical Engineers.
[24] Moretti, G., Rosati, G. P. P., Alves, M., Grases, M., Vertechy, R., & Fontana, M. (2015, May). Analysis and design of an oscillating water column wave energy converter with dielectric elastomer power take-off. In International Conference on Offshore Mechanics and Arctic Engineering (Vol. 56574, p. V009T09A023). American Society of Mechanical Engineers.